Dyes and Pigments 95 (2012) 639–643

Contents lists available at SciVerse ScienceDirect

Dyes and Pigments

journal homepage: www.elsevier.com/locate/dyepig

Preparation, microstructure, and color tone of microtubule material composed of hematite/amorphous-silicate nanocomposite from iron oxide of bacterial origin

Hideki Hashimoto [a], Hiroshi Asaoka [a], Takuya Nakano [a], Yoshihiro Kusano [b], Hiromichi Ishihara [a], Yasunori Ikeda [c], Makoto Nakanishi [a], Tatsuo Fujii [a], Tadanori Yokoyama [d], Nanao Horiishi [e], Tokuro Nanba [f], Jun Takada [a,*]

[a] Graduate School of Natural Science and Technology, Okayama University, Okayama 700-8530, Japan
[b] Department of Fine & Applied Arts, Kurashiki University of Science and the Arts, Kurashiki, Okayama 712-8508, Japan
[c] Research Institute for Production Development, Sakyo-ku, Kyoto 606-0805, Japan
[d] Kyoto Municipal Institute of Industrial Technology and Culture, Kyoto 600-8815, Japan
[e] Bengala Techno Lab, Kawasaki, Kanagawa 216-0007, Japan
[f] Graduate School of Environmental Science, Okayama University, Okayama 700-8530, Japan

ARTICLE INFO

Article history:
Received 17 May 2012
Received in revised form
27 June 2012
Accepted 27 June 2012
Available online 6 July 2012

Keywords:
Iron-oxidizing bacteria
Biogenous iron oxides
Microtubule
Nanocomposite
Hematite
Amorphous silicate

ABSTRACT

By heating an amorphous iron oxide produced by *Leptothrix ochracea*, an iron-oxidizing bacterium species, at 600–1100 °C in air for 2 h, vivid red-colored powdered materials including α-Fe_2O_3 (hematite) and amorphous silicate with high thermostability were prepared which offer potential for use as overglaze enamels on porcelain. The precise color tone of the materials greatly depends on the heat-treatment temperature. The most strikingly beautiful sample, heat-treated at 800 °C, is light yellowish-red in color ($L^* = 47.3$, $a^* = 34.1$, and $b^* = 34.6$), has a unique microstructure, and does not fade in color even with reheating at 800 °C, which is the firing temperature for overglaze enamel on porcelain. The sample primarily consists of crystalline hematite particles ~40 nm in diameter with slightly longer axis unit-cell parameters than those of pure hematite. The particles are covered with amorphous silicate phase ~5 nm in thickness and are intricately interconnected into microtubules with an average diameter of 1.26 μm. The attractive color of this material is due to the following structural features: small particle size (~40 nm), nanocomposite of hematite and amorphous silicate, and a microtubule structure that inhibits aggregation of individual hematite particles and microtubules.

1. Introduction

Hematite is of significant interest to nanoscience and nanotechnology researchers because of its potential for application in pigments, gas-sensing materials, catalysts, and positive and negative electrodes of lithium-ion batteries [1–14]. In recent years, many synthetic routes to hematite nanoparticles have been reported, such as the hydrolysis of an Fe (III) solution, thermal decomposition, sol–gel methods, and microemulsion methods [15–17]. Important requirements for these synthetic routes are the capability to control particle size, distribution, dispersibility, and morphology at the nanometer level.

Because of its beautiful color, hematite powder is widely used as a pigment for overglaze enamels on porcelain. By "beautiful color," we mean that the color exhibits high L^*, a^*, and b^* values on a CIE 1976 $L^*a^*b^*$ color space [18]. In Japan, vivid yellowish-red hematite has been used in an elegant enamel-decoration technique called *aka-e*, commonly performed on the milk-white body of Kakiemon-style ware with a simplified design scheme using sufficient space. Kakiemon-style ware enthralled royalty and aristocrats when it was exported to Europe in the 17th and 18th centuries [19–23], and continues to revere by admirers worldwide.

In general, hematite color increases in beauty with decreasing particle size [24–26]. When hematite is used in *aka-e*, the overglaze enamel is prepared by mixing hematite powder, appropriate glazes, and solvents, drawing with this mixture on porcelain, and then heat-treating the porcelain at high temperature (~800 °C) to fix the overglaze enamel onto the porcelain body [27]. A common problem with hematite from natural ores and industrially synthesized hematite, both of which are used widely in red-overglaze enamels, is that their color fades when the hematite grain growth occurs under heat treatment. Therefore, it is highly desirable for hematite powder to not only be beautiful in color but also be thermostable and not be susceptible to grain growth during heat

* Corresponding author. Tel.: +81 862518107; fax: +81 862518087.
E-mail address: jtakada@cc.okayama-u.ac.jp (J. Takada).

0143-7208/$ – see front matter © 2012 Elsevier Ltd. All rights reserved.
http://dx.doi.org/10.1016/j.dyepig.2012.06.024

treatment for its use as overglaze enamels. Chemical stability of hematite powder in molten glazes is also an important factor. Recently in order to add thermostability and chemical stability to pigments, heteromorphic pigments which are composites of colored crystal and stable uncolored phase (e.g., composite of hematite and silica) have been developed and their excellent properties have been reported [4–9]. In this study we propose a new synthetic route for thermostalbe red powder including hematite and amorphous silicate using iron oxide with microtubular form produced by iron-oxidizing bacteria (FeOB) as a starting material.

In natural aquatic environments, FeOB gain energy for survival by oxidizing ferrous ions to ferric oxides. Micrometer-scale iron oxides of various shapes are produced by different FeOB species and are visible everywhere as ocher precipitates [28–32] that have until now been regarded as unwanted nuisances. Our collective term for iron-containing precipitates formed by FeOB is biogenous iron oxides (BIOXs).

To date, most relevant BIOXs studies have been conducted from microbiological and geochemical perspectives [28–40]. However, we have conducted studies from a materials-science perspective and reported various important features of BIOXs [41–45]. The target BIOX in this study is BIOX with microtubular form (*L*-BIOX) formed by the most well-known FeOB *Leptothrix ochracea* [30]. We previously reported that *L*-BIOX is a porous iron oxide with a unique structure, consisting of primary particles ~3 nm in diameter aggregated into secondary particles several tens of nanometer in diameter and finally into a microtubule ~1 μm in diameter [41,42]. The iron oxide particles have low crystalline features of chemical composition Fe:Si:P = 73:22:5 with the exception of O, H, and C [43]. Surprisingly, we discovered that the natural enzyme lipase immobilized on *L*-BIOX exhibits high catalytic activity [42].

More recently, by using *L*-BIOX as a starting material, we prepared a powder material including hematite and amorphous silicate with beautiful yellowish-red color. Its particles did not grow and fade in color even at 800 °C. Here, we report its microstructure in detail, focusing especially on the existence of an amorphous phase, and consider the effects of the microstructure on color tone.

2. Experimental

L-BIOX was collected from an enrichment culture tank and centrifuge-washed with distilled water several times to remove impurities, as described in our previous reports [41,43,44]. The washed *L*-BIOX was dried at 100 °C in air, heat-treated at 600–1100 °C (every 100 °C) in air for 2 h at a heating rate of 10 °C/min, and allowed to cool in the furnace. The resulting powders were analyzed by X-ray diffractometry (XRD; Rigaku RINT-2000).

The sample heat-treated at 800 °C (monophasic hematite in terms of XRD) was evaluated by high-resolution transmission electron microscopy (HRTEM; JEOL JEM-2100F) and scanning electron microscopy (SEM; Hitach S-4300) equipped with energy-dispersive X-ray spectroscopy (EDS; JEOL JED-2300T and EDAX Genesis 2000, respectively) and colourimetry with a standard illuminant of D_{65} (Konica Minolta Sensing CM-2600d). Commercially available hematite (Morishita Bengara Kogyo MC-55) which is used as a red pigment for overglaze enamels on porcelain bodies was used as a reference color-tone sample. For studying the thermostability of the powder color, both the sample that was heat-treated at 800 °C and MC-55 were heat-treated at 800 °C for 1 h in air, and the colors were evaluated. The average particle sizes and their standard deviation values described in this paper were estimated by measuring at least 70 particles on SEM or TEM images.

3. Results and discussion

Fig. 1 shows photographs and XRD patterns of *L*-BIOX and the heat-treated powder samples. The color tone of the heat-treated samples greatly depends on the heat-treatment temperature. *L*-BIOX is ocher (Fig. 1a), while the heat-treated samples range from brown (600 and 700 °C, Fig. 1b and c) to yellowish-red (800 °C, Fig. 1d), wine red (900 °C, Fig. 1e), purple (1000 °C, Fig. 1f), and finally black (1100 °C, Fig. 1g). The color change from ocher or brown to red is well known to accompany the phase transformation from iron oxyhydroxide (FeOOH) to hematite. Common iron oxyhydroxides transform easily to hematite near 300 °C, while *L*-BIOX does not undergo a phase transformation even at 600 °C (Fig. 1i), indicating the difficulty of phase transformation to hematite in the case of *L*-BIOX. *L*-BIOX slightly crystallizes to hematite at 700 °C (Fig. 1j), and transforms to monophasic hematite at 800 °C (Fig. 1k). According to our previous report, *L*-BIOX contains structural Si and P with a relative composition of Fe:S:P = 73:22:5 [43]. This composition dose not change with heat treatment in air, as we confirmed by SEM-EDS. The existence of structural Si and P in *L*-BIOX could inhibit the rearrangement of ions during heat treatment, significantly raising the transformation temperature to hematite. Further, after heat treatment at ≥900 °C (Fig. 1l–n), crystalline silica (cristobalite) and iron phosphate (rodolicoite and/or grattarolaite) form. Formation of cristobalite suggests that the sample heat-treated at <900 °C, namely 800 °C, could contain amorphous silica [46]. Additionally, diffraction peaks of hematite at ≥800 °C sharpen with increasing temperature (Fig. 1k–n), indicating that the crystallite size has increased (e.g., 25, 80, and 139 nm at 800, 900, and 1000 °C, respectively, calculated by the

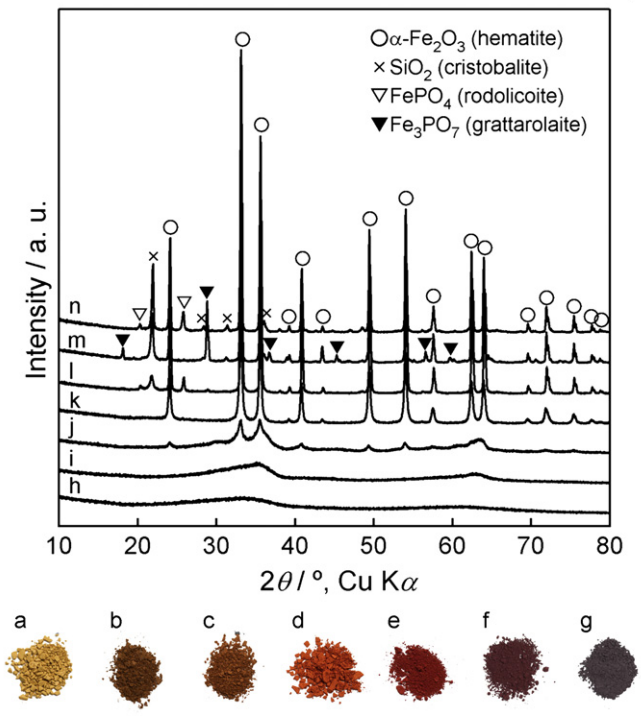

Fig. 1. (a) Photograph and (h) XRD pattern of dried *L*-BIOX. Two broad peaks at the *d*-spacing values of 0.27 and 0.15 nm were observed. (b–g) Photographs and (i–n) XRD patterns of the samples heat treated at 600, 700, 800, 900, 1000, and 1100 °C, respectively. *L*-BIOX showed various color depending on the heat-treatment temperature. The Bragg reflections of hematite appeared at ≥700 °C. Hematite with lattice parameters of $a = 0.5039$, and $c = 1.3767$ nm was produced at 800 °C. Crystalline silica and iron phosphate were produced at ≥900 °C.

Scherrer equation using (104) plane). We note that the sample that was heat-treated at 800 °C (*L*-800) is monophasic hematite in terms of XRD with a light yellowish-red color.

The unit-cell parameters of *L*-800 are $a = 0.5039$ nm and $c = 1.3767$ nm, which are slightly longer than those of pure hematite ($a = 0.50356$, $c = 1.37489$ nm [47]). Campbell et al. suggested that structural OH and/or Si within the hematite structure can cause the Fe occupancy to decrease consistently, and thus changing the hematite lattice parameters [48]. Gálvez et al. prepared hematite with structural P and reported that the *c*-axis length increases with increasing P content, with P occupying tetrahedral sites in the hematite structure [49]. Therefore, we speculate that the unit-cell parameters of *L*-800 are slightly longer than those of pure hematite, because small amounts of Si^{4+} and/or P^{5+} ions could be located randomly at some tetrahedral sites surrounded by oxygen ions in the hematite crystal structure.

Fig. 2 shows color measurements for untreated *L*-800, untreated commercially available hematite (MC-55, particle size 104 ± 20 nm), heat-treated *L*-800, and heat-treated MC-55; heat treatment was performed at 800 °C for 1 h and the resulting samples are denoted Re-*L*-800 and Re-MC-55. The reflectance edge of each sample is in the same position approximately, near 585 nm, but reflectance intensities beyond 450 nm decrease in the following order: *L*-800 ≈ Re-*L*-800 > MC-55 > Re-MC-55 (Fig. 2a). In Fig. 2b, the CIE parameters L^* (lightness), a^* (reddish) and b^* (yellowish), derived from reflectance curves, indicate that MC-55 has the highest a^* value (35.2), but *L*-800, with its beautiful light yellowish-red color and the values $L^* = 47.3$, $a^* = 34.1$ and $b^* = 34.6$, has the highest b^* and L^* values. Furthermore, the values for Re-*L*-800 (heat-treated) are almost equal to those for *L*-800 (unheated), while Re-MC-55 shows significant color fading with the values $L^* = 39.1$, $a^* = 28.8$, $b^* = 17.5$ (Fig. 2b). These results indicate that *L*-800 is a thermostable hematite powder with high CIE values.

In general, the color of hematite powder depends on its particle size and aggregation state and ranges from vivid red for small, dispersive particles to black for large, aggregated particles [24–26]. Accordingly, Re-MC-55 (dull red) would seem to have large particle sizes, while Re-*L*-800 (vivid red) would seem to have maintained its original particle size. SEM and TEM observations show that the average particle size of Re-MC-55 is 196 ± 54 nm, twice that of MC-55 (measured by SEM), while the average particle size of Re-*L*-800 is 36 ± 14 nm, the same as that of *L*-800 (measured by TEM).

Fig. 3 shows TEM images of *L*-BIOX and *L*-800, which we obtained to clarify the reason for *L*-800's beautiful color. *L*-BIOX particles are intricately interconnected into microtubules. The electron diffraction (ED) pattern of a single microtubule shows a halo, indicating an almost amorphous structure (Fig. 3a). *L*-800 particles maintain their tubular shape even after exposure to high temperature, and the ED pattern of a microtubule shows the ring pattern of polycrystalline hematite (Fig. 3b). The outer diameter of *L*-BIOX shrinks with heat treatment from 1.35 μm to 1.26 μm (shrinking ratio 7%). HRTEM observation shows that *L*-BIOX is amorphous and exhibits granular particle morphology (Fig. 3c), while *L*-800 has crystallized to hematite (diameter 36 ± 17 nm, ranging from 8 to 98 nm), and the hematite particles are covered with an amorphous phase (thickness was ranging from 1 to 21 nm) (Fig. 3d). The morphologies and sizes of these crystals and the amorphous phase are heterogeneous. Si and O are mainly detected from the amorphous phase by EDS point analysis, indicating that the amorphous phase belongs to an amorphous silicate. These careful observations revealed that the simple heat-treatment of *L*-BIOX can give complicated nano- and micro-architectural structure material (microtubule material composed of hematite/amorphous-silicate nanocomposite). This complicated microstructure could

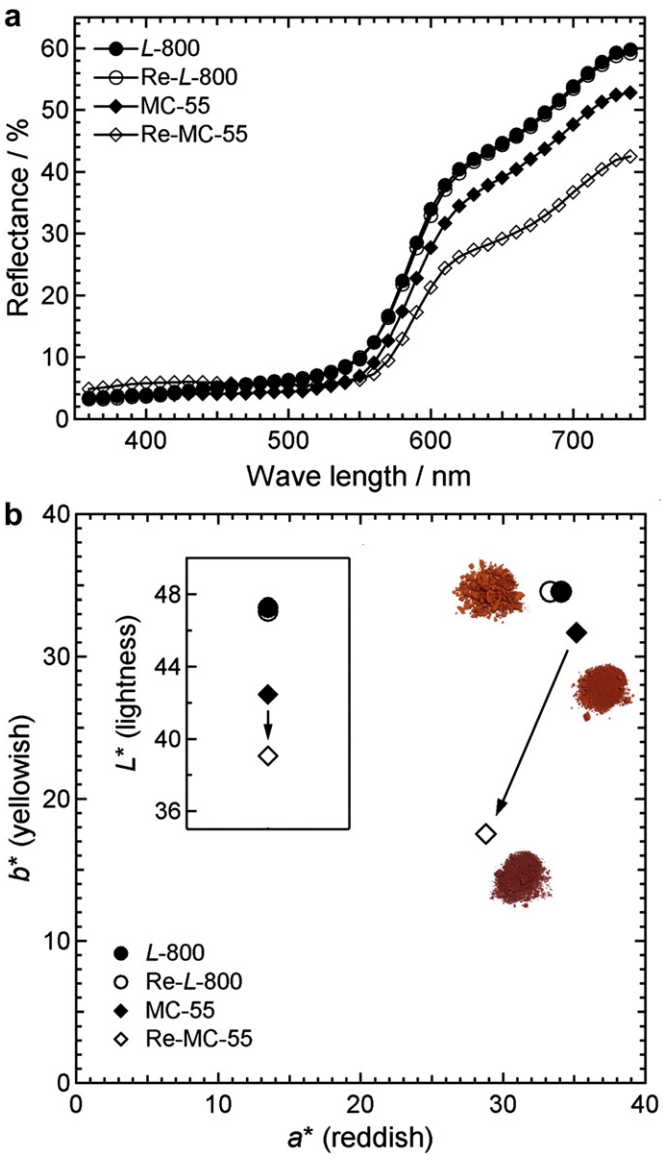

Fig. 2. (a) Reflectance curves of *L*-800, Re-*L*-800, MC-55, and Re-MC-55. (b) L^* (inset), a^*, and b^* values of the samples. *L*-800 maintained a vivid red color under heat treatment of 800 °C, while MC-55 showed significant color fading. The inset photographs are powders of *L*-800, MC-55, and Re-MC-55. CIE 1976 $L^*a^*b^*$ color space. L^* indicates lightness, and a^* and b^* indicate chromaticity, i.e., color directions. Positive and negative values of a^* indicate reddish and greenish color, respectively, whereas positive and negative values of b^* indicate yellowish and bluish color, respectively.

contribute to *L*-800's beautiful color and thermostability mentioned as follows.

Previous reports showed that hematite with small, dispersive particles has a beautiful color [24–26] and that silica-coating of hematite enhances its hue [4–9]. Three factors in particular seem to contribute to the beautiful color: small particle size (~40 nm), presence of an amorphous silicate shell, and a tubular structure that inhibits the aggregation of individual hematite particles and microtubules. As evidence of the importance of the third factor, when we crushed *L*-800 with an alumina mortar to break the tubules, the crushed sample faded in color ($L^* = 42.2$, $a^* = 33.1$, and $b^* = 33.2$).

The process of phase separation during heat treatment of *L*-BIOX deserves further consideration. We previously reported

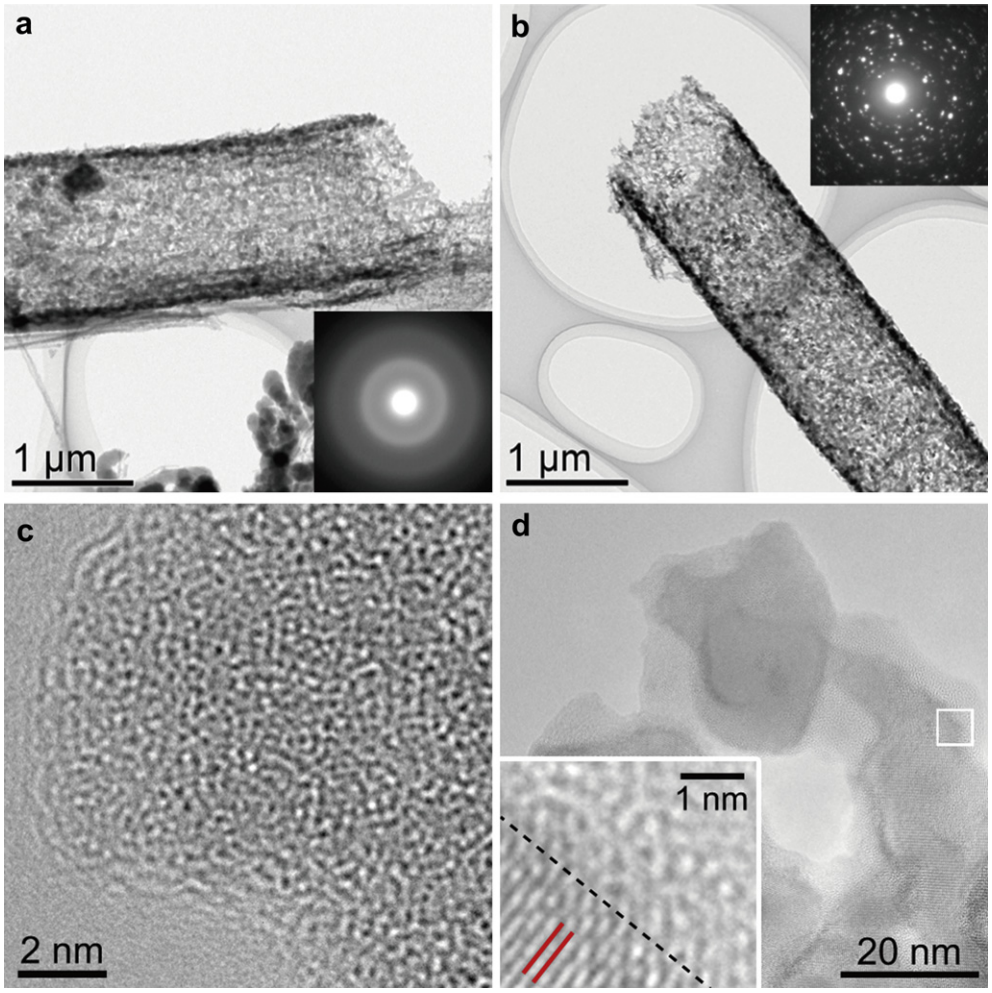

Fig. 3. TEM images of (a, c) *L*-BIOX and (b, d) *L*-800. Inset images in (a) and (b) are electron diffraction patterns. Inset to (d) is the magnified image of white square area and solid lines show the (113) plane of hematite. The dotted line shows the boundary between hematite and amorphous silicate.

that *L*-BIOX has chemical bonds of Fe–O–Si [44]. During heat treatment, thermal energy can accomplish the following three objectives: (1) it can break the Fe–O–Si bonds; (2) it can rearrange the ions and nucleate the hematite crystals, resulting in a phase separation into two phases of hematite and amorphous silicate; and (3) it can cause hematite grain growth. Phosphorus is well known to promote phase separation in glass [50], which suggests that observed phase-separation process may be promoted by phosphorus. Further investigations concerning spatial distribution of Si, O, P, and Fe in the amorphous silicate phase are in progress.

The possibility of relationships of *L*-800's slightly longer unit-cell parameters relative to those of pure hematite with color tones should be pointed out as follows. Gálvez et al. reported that structural P contributing to Fe deficiency in the hematite structure changes the intensity of the absorption bands of Fe^{3+} ligand field transition in the visible region [49]. Pailhé et al. reported that the reduction of the octahedral distortion that causes Fe^{3+} sites to move from O_h to D_{3d} and C_{3v} is directly correlated with the two Fe–O charge-transfer bands in the visible range and with the color of hematite [3]. These reports suggest that *L*-800's slightly longer unit-cell parameters relative to those of pure hematite could affect its color. Among subjects for future study are the amounts of structural Si and/or P, their atomic sites, degree of the octahedral distortion, and the relationship between these phenomena and color.

4. Conclusions

We prepared various colored powders by heating *L*-BIOX at 600–1100 °C. We selected the most beautiful powder, the one that was heat-treated at 800 °C, for more detailed investigation. It has a complicated microstructure that primarily consists of crystalline hematite nanoparticles ~40 nm in diameter, with unit-cell parameters slightly longer than those of pure hematite. The nanoparticles are covered with amorphous silicate ~5 nm in thickness and are intricately interconnected into microtubules with an average diameter of 1.26 μm. Such a complicated structure would be difficult to synthesize artificially, but is easy to produce by simple heat treatment using *L*-BIOX as a starting material. Interestingly, the resulting product is a more beautiful yellowish-red color that is more thermostable than that of commercially available hematite. We propose the following three reasons for the beautiful color; (1) the hematite particles are small (~40 nm); (2) amorphous silicate forms on the surface of the particles; and (3) the particles are intricately interconnected into microtubules that inhibit aggregation of individual hematite particles and microtubules. We believe that *L*-800 powder has great potential as a vivid red pigment for overglaze enamels on porcelain.

Acknowledgments

This study was financially supported by the Special Grant for Education and Research from the Ministry of Education, Culture,

Sports, Science, and Technology, Japan (for J. T.) and the Grant-in-Aid Research Activity Start-up (No. 22860040, 2010 and 2011, H.H).

References

[1] Katsuki H, Komarneni S. Microwave-hydrothermal synthesis of monodispersed nanophase α-Fe_2O_3. J Am Ceram Soc 2001;84(10):2313–7.
[2] Katsuki H, Komarneni S. Role of α-Fe_2O_3 morphology on the color of red pigment for porcelain. J Am Ceram Soc 2003;86(1):183–5.
[3] Pailhé N, Wattiaux A, Gaudon M, Demourgues A. Impact of structural features on pigment properties of α-Fe_2O_3 haematite. J Solid State Chem 2008;181(10):2697–704.
[4] Bondioli F, Ferrari AM, Leonelli C, Manfredini T. Synthesis of Fe_2O_3/Silica red inorganic inclusion pigments for ceramic applications. Mater Res Bull 1998;33(5):723–9.
[5] Hosseini-Zori M, Taheri-Nassaj E, Mirhabibi AR. Effective factors on synthesis of the hematite–silica red inclusion pigment. Ceram Int 2008;34(3):491–6.
[6] Hosseinizori M, Bondioli F, Manfredini T, Taherinassaj E. Effect of synthesis parameters on a hematite–silica red pigment obtained using a coprecipitation route. Dyes Pigments 2008;77(1):53–8.
[7] Zhang Y, Rao P, Lü M, Zeng D, Wu J. Synthesis and color evolution of silica-coated hematite nanoparticles. J Am Ceram Soc 2009;92(8):1877–80.
[8] Yu R, Kim Y, Pee JH, Kim KJ, Kim W. Thermal behavior and coloration study of silica-coated α-Fe2O3 and β-FeOOH nanocapsules. J Nanosci Nanotechno 2011;11(7):6283–6.
[9] Hosseini-Zori M, Taheri-Nassaj E. Nano encapsulation of hematite into silica matrix as a red inclusion ceramic pigment. J Alloys Compd 2012;510(1):83–6.
[10] Huo L, Li W, Lu L, Cui H, Xi S, Wang J, et al. Preparation, structure, and properties of three-dimensional ordered α-Fe_2O_3 nanoparticulate film. Chem Mater 2000;12(3):790–4.
[11] Chen J, Xu L, Li W, Gou X. α-Fe_2O_3 nanotubes in gas sensor and lithium-ion battery applications. Adv Mater 2005;17(5):582–6.
[12] Wagloehner S, Reichert D, Leon-Sorzano D, Balle P, Geiger B, Kureti S. Kinetic modeling of the oxidation of CO on Fe_2O_3 catalyst in excess of O_2. J Catal 2008;260(2):305–14.
[13] Komaba S, Suzuki K, Kumagai N. Synthesis of nanocrystalline Fe_2O_3 for lithium secondary battery cathode. Electrochemistry 2002;70(7):506–10.
[14] Hang BT, Okada S, Yamaki J-i. Effect of binder content on the cycle performance of nano-sized Fe_2O_3-loaded carbon for use as a lithium battery negative electrode. J Power Sources 2008;178(1):402–8.
[15] Matijevic E, Scheiner P. Ferric hydrous oxide sols: III. Preparation of uniform particles by hydrolysis of Fe (III)-chloride, -nitrate, and-perchlorate solutions. J Colloid Interface Sci 1978;63(3):509–24.
[16] Sugimoto T, Wang Y, Itoh H, Muramatsu A. Systematic control of size, shape and internal structure of monodisperse α-Fe_2O_3 particles. Colloids Surf Physicochem Eng Aspects 1998;134(3):265–79.
[17] Han L-H, Liu H, Wei Y. In situ synthesis of hematite nanoparticles using a low-temperature microemulsion method. Powder Technol 2011;207(1–3):42–6.
[18] Ohno Y. CIE fundamentals for color measurements. In: paper for IS&T NIP16 conference. Canada: Oct. 2000, vols. 16–20. p. 1–6.
[19] Hidaka M, Ohashi K, Kajihara S, Wijesundera R, Kumara L, Choi J, et al. Structural properties of the red-color overglaze for the HIZEN porcelains produced in the early Edo period of Japan. Ceram Int 2009;35(2):875–86.
[20] Hidaka M, Horiuchi H, Ohashi K, Wijesundera R, Kumara L, Choi JY, et al. Structural properties of the red-color overglazes on the kakiemon-style porcelains produced in the later 17th century by means of X-ray diffraction (I). Cerâmica 2009;55(334):120–7.
[21] The Kyushu Ceramic Museum. Commemorative exhibition of the Shibata donation: Shibata collection VIII: the splendor of Ko-Imari. Sanko Co. Ltd; 2002.
[22] Schiffer NN. Imari Satsuma and other Japanese export ceramics. 2nd ed. Schiffer Publishing Ltd; 2000.
[23] Shimura G. The story of Imari: the symbols and mysteries of Antique Japanese porcelain. Ten Speed Press; 2008.
[24] Takada T. On the effects of particle size and shape on the colour of ferric oxide powders. J Jpn Soc Powder Powder Metall 1958;4:160–8.
[25] Kusano Y, Fukuhara M, Takada J, Doi A, Ikeda Y, Takano M. Science in the art of the master Bizen potter. Acc Chem Res 2010;43(6):906–15.
[26] Cornell RM, Schwertmann U. The iron oxides: structure, properties, reactions, occurrences, and uses. Willey-VCH; 2003.
[27] The Kyushu Ceramic Museum. Earth and fire: the historical development of Kyushu ceramics. Sanko Co., Ltd; 1996.
[28] Ghiorse WC. Biology of iron and manganese-depositing bacteria. Annu Rev Microbiol 1984;38:515–50.
[29] Emerson D, Fleming EJ, McBeth JM. Iron-oxidizing bacteria: an environmental and genomic perspective. Annu Rev Microbiol 2010;64:561–83.
[30] Spring S. The genera Leptothrix and Sphaerotilus. In: Dworkin M, Falkow S, Rosenberg E, Schleifer KH, Stackebrandt E, editors. The prokaryotes. New York: Springer; 2006. p. 758–77.
[31] Hanert HH. The genus Gallionella. In: Dworkin M, Falkow S, Rosenberg E, Schleifer KH, Stackebrandt E, editors. The prokaryotes. New York: Springer; 2006. p. 990–5.
[32] Hirsch P. The genus Toxothrix. In: Dworkin M, Falkow S, Rosenberg E, Schleifer KH, Stackebrandt E, editors. The prokaryotes. New York: Springer; 2006. p. 986–9.
[33] Emerson D, Moyer C. Isolation and characterization of novel iron-oxidizing bacteria that grow at circumneutral pH. Appl Environ Microbiol 1997;63(12):4784–92.
[34] Emerson D, Revsbech NP. Investigation of an iron-oxidizing microbial mat community located near Aarhus, Denmark: laboratory studies. Appl Environ Microbiol 1994;60(11):4032–8.
[35] Banfield JF, Welch SA, Zang H, Ebert TT, Penn RL. Aggregation-based crystal growth and microstructure development in natural iron oxyhydroxide biomineralization products. Science 2000;289(5480):751–4.
[36] Chan CS, De Stasio G, Welch SA, Girasole M, Frazer BH, Nesterova MV, et al. Microbial polysaccharides template assembly of nanocrystal fibers. Science 2004;303(5664):1656–8.
[37] Ferris FG. Biogeochemical properties of bacteriogenic iron oxides. Geomicrobiol J 2005;22(3–4):79–85.
[38] Ferris FG, Konhauser KO, Lyven B, Pedersen K. Accumulation of metals by bacteriogenic iron oxides in a subterranean environment. Geomicrobiol J 1999;16(2):181–92.
[39] Mouchet P. From conventional to biological removal of iron and manganese in France. J Am Water Works Assn 1992;84(4):158–67.
[40] Katsoyiannis IA, Zouboulis AI. Biological treatment of Mn(II) and Fe(II) containing groundwater: kinetic considerations and product characterization. Water Res 2004;38(7):1922–32.
[41] Hashimoto H, Yokoyama S, Asaoka H, Kusano Y, Ikeda Y, Seno M, et al. Characteristics of hollow microtubes consisting of amorphous iron oxide nanoparticles produced by iron oxidizing bacteria, *Leptothrix ochracea*. J Magn Magn Mater 2007;310(2):2405–7.
[42] Ema T, Miyazaki Y, Kozuki I, Sakai T, Hashimoto H, Takada J. Highly active lipase immobilized on biogenous iron oxide via an organic bridging group: the dramatic effect of the immobilization support on enzymatic function. Green Chem 2011;13(11):3187–95.
[43] Suzuki T, Hashimoto H, Ishihara H, Kasai T, Kunoh H, Takada J. Structural and spatial associations between Fe, O, and C in the network structure of the *Leptothrix ochracea* sheath surface. Appl Environ Microbiol 2011;77(21):7873–5.
[44] Takada J, Fujii T, Nakanishi M. Jpn Patent Kokai 2008:177061 [31.07.08].
[45] Suzuki T, Hashimoto H, Matsumoto N, Furutani M, Kunoh H, Takada J. Nanometer-scale visualization and structural analysis of the inorganic/organic hybrid structure of *Gallionella ferruginea* twisted stalks. Appl Environ Microbiol 2011;77(9):2877–81.
[46] Hamad M, Khattab I. Effect of the combustion process on the structure of rice hull silica. Thermochim Acta 1981;48(3):343–9.
[47] PDF 00-033-0664 (ICDD, 2009).
[48] Campbell A, Schwertmann U, Stanjek H, Friedl J, Kyek A, Campbell P. Si incorporation into hematite by heating Si-ferrihydrite. Langmuir 2002;18(21):7804–9.
[49] Galvez N, Barron V, Torrent J. Preparation and properties of hematite with structural phosphorus. Clays Clay Miner 1999;47(3):375–85.
[50] Rabinovich EM, Ish-Shalom M, Kisilev A. Metastable liquid immiscibility and vycor-type glass in phosphate–silicate systems. J Mater Sci 1980;15(8):2027–38.